2019 IEEE 58th Conference on Decision and Control (CDC)
Palais des Congrès et des Expositions Nice Acropolis
Nice, France, December 11-13, 2019

Some Remarks on Robust Gene Regulation in a Biomolecular Integral Controller

Deepak K. Agrawal, Ryan Marshall, M. Ali Al-Radhawi, Vincent Noireaux, and Eduardo D Sontag

Abstract— **Integral feedback can help achieve robust tracking independently of external disturbances. Motivated by this knowledge, biological engineers have proposed various designs of biomolecular integral feedback controllers to regulate biological processes. In this paper, we theoretically analyze the operation of a particular synthetic biomolecular integral controller, which we have recently proposed and implemented experimentally. Using a combination of methods, ranging from linearized analysis to sum-of-squares (SOS) Lyapunov functions, we demonstrate that, when the controller is operated in closed-loop, it is capable of providing integral corrections to the concentration of an output species in such a manner that the output tracks a reference signal linearly over a large dynamic range. We investigate the output dependency on the reaction parameters through sensitivity analysis, and quantify performance using control theory metrics to characterize response properties, thus providing clear selection guidelines for practical applications. We then demonstrate the stable operation of the closed-loop control system by constructing quartic Lyapunov functions using SOS optimization techniques, and establish global stability for a unique equilibrium. Our analysis suggests that by incorporating effective molecular sequestration, a biomolecular closed-loop integral controller that is capable of robustly regulating gene expression is feasible.**

I. INTRODUCTION

Genetic networks often require maintaining a stable equilibrium in the presence of biological disturbances. Feedback provides a mechanism to achieve this goal. It has been shown that feedback in transcriptional networks can work autonomously to maintain homeostasis independent of exogenous or endogenous disturbances [1]–[5]. This has led to the development of integral controllers that use negative feedback to correct the concentration of an output species to provide robust tracking [6]–[10]. In this work, we analyze the operation of a synthetic biomolecular integral controller designed to robustly regulate gene expression, which we recently proposed and experimentally implemented [6], based on sigma and anti-sigma factors. Our controller uses molecular sequestration to calculate the error between the set-point, i.e. reference, and the output species, an architecture introduced by Briat, Gupta, and Khammash [7]. A sigma factor regulator is employed in a feedback pathway to precisely control the expression of an output species, in such a manner that the output species can follow changes in the reference signal autonomously in the presence of known disturbances [6].

Specifically, we investigate the operation of the controller through a combination of numerical and analytical techniques, similar to [8], on an ordinary differential equation (ODE) model that we recently developed [6]. The controller presented in [6] is superior to the one in [8] because it uses protein a molecular-based sequestration reaction, which is more effective than RNA based sequestration reactions. We compare the controller's open- and closed-loop operation in their capacity to guarantee that an output species can accurately follow significant changes in a reference signal linearly, even if the kinetic rates are perturbed or a disturbance is added. Using steady-state analysis and time-scale separation, we derive analytical equations of the controller's output that provide insight into which parameters govern the steady-state output dynamics.

Moreover, we ask about the effect of step input disturbances after a steady-state has been achieved, and investigate the robustness of the controller to changes in the input. We carry out a sensitivity analysis to explore the influence of parameter variability on the output dynamics when the input undergoes a step change. We then use traditional control theory metrics to evaluate the performance of the controller at different reaction conditions. We also study the local and the global stability of the controller. In particular, using sum-of-squares optimization techniques, we demonstrate that the dynamics of our closed-loop controller is stable at an equilibrium point, and the controller output always converges to a steady-state for any input value. This computational study serves as a guide in the design of a biomolecular integral controller for robust and precise regulation of gene expression. In a more general context, our work highlights mathematical tools that might be useful in the analysis of other biomolecular systems.

Our approach involves a traditional closed-loop integral controller architecture [6], [11], as classically done for robust tracking. In this approach, sensors and actuators are interconnected to achieve a closed-loop operation where the output and the input are compared through error computation to achieve reference tracking while the mathematical integral of the error signal enables rejection to certain kinds of disturbances in the steady-state output dynamics [12]. The biomolecular design of the closed-loop controller uses three genes P_X, P_Y and P_Z that encode for X, Y and Z proteins respectively. The concentration of gene P_X is used to set a

Deepak K. Agrawal, M. Ali Al-Radhawi, and Eduardo D Sontag are with the Department of Bioengineering, and Department of Electrical and Computer Engineering, Northeastern University, Boston, MA 02115, USA agwal.deepak@gmail.com, {malirdwi,e.sontag}@northeastern.edu

Ryan Marshall, and Vincent Noireaux are with the School of Physics and Astronomy, University of Minnesota, Minneapolis, MN 55455, USA marsh752@umn.edu, noireaux@umn.edu

E. Sontag is with the Laboratory of Systems Pharmacology, Program in Therapeutic Science, Harvard Medical School, Boston, MA, USA

978-1-7281-1398-2/19/$31.00 ©2019 IEEE

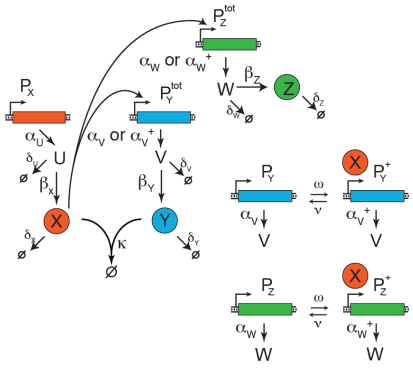

Fig. 1. Detailed reaction network of the controller. Here U, V and W are the translationally initiated mRNAs of the X, Y and Z proteins respectively. Details on how the P_Y^{tot} and P_Z^{tot} promoters switch from the inactive (P_Y, P_X) to active (P_Y^+, P_Z^+) states are shown alongside.

reference, and the controller regulates expression of gene P_Z by influencing its promoter activity (Fig. I). Gene P_Y is used as a proxy to represent gene P_Z. We used transcription and translation reactions as a signal-transduction mechanism: the constitutive gene P_X produces X, and the regulated genes P_Y and P_Z produce Y and Z respectively (Fig. I). When activated, genes P_Y and P_Z switch to their active states P_Y^+ and P_Z^+, respectively, transcribing Y and Z faster than the inactive state.

Feedback is introduced via molecular sequestration that serves as an error computation [6], [7]. For that purpose, X and Y protein molecules are used, which represent input and output respectively, in such a manner that once X and Y bind to each other, they form a waste complex that is not involved in any other reaction in the system. As a result of the sequestration reaction, only the excess molecules of X that did not bind to Y yield an error signal that is available for control reactions. Non-sequestered X is used directly as a transcriptional activator that regulates the production of Y and Z (Fig. I). To ensure that Y truly represents the output Z, the same promoter should be used by the genes P_Y and P_Z. In the open-loop configuration, the error computation is absent and to achieve that, gene P_Y is set to zero so that Y (required for the error computation) will not be expressed.

A. Mathematical Analysis

Using mass-action kinetics, the controller can be modeled as [6]:

$$\dot{U} = \alpha_U P_X - \delta_U U, \tag{1}$$

$$\dot{X} = \beta_X U - \kappa XY - \delta_X X - \omega X P_Y \ldots + \nu P_Y^+ - \omega X P_Z + \nu P_Z^+, \tag{2}$$

$$\dot{P_Y^+} = \omega X P_Y - \nu P_Y^+, \tag{3}$$

$$\dot{V} = \alpha_V P_Y + \alpha_V^+ P_Y^+ - \delta_V V, \tag{4}$$

$$\dot{Y} = \beta_Y V - \kappa XY - \delta_Y Y, \tag{5}$$

$$\dot{P_Z^+} = \omega X P_Z - \nu P_Z^+, \tag{6}$$

$$\dot{W} = \alpha_W P_Z + \alpha_W^+ P_Z^+ - \delta_W W, \tag{7}$$

$$\dot{Z} = \beta_Z W - \delta_Z Z, \tag{8}$$

where $\dot{}$ represents time derivative. Here, α, β and δ in general are the transcription, translation and degradation rate constants with subscripts indicting the corresponding species respectively, while κ is the sequestration rate constant, ω and ν are the activation association and dissociation rate constants respectively. When the activator (X) binds at the promoter region of genes P_Y and P_Z, Y and Z are produced with increased rates, denoted as α_V^+ and α_W^+ respectively. The activated states of genes P_Y and P_Z are represented as P_Y^+ and P_Z^+, and the conservation law $P_Y^{tot} = P_Y + P_Y^+$ and $P_Z^{tot} = P_Z + P_Z^+$ holds. For robust tracking, $\kappa XY \gg \delta_X X$, $\kappa XY \gg \delta_Y Y$, $\alpha_V^+ \gg \alpha_V$, $\alpha_W^+ \gg \alpha_W$, and $P_Y^{tot} = P_Z^{tot}$ should be true when $X > 0$ and $Y > 0$ [6], [8].

1) Open-loop steady-state output: To understand the operation of the controller, we first derive the steady-state expression of the output in the open-loop configuration. As gene P_Y is absent, we can ignore (3) (4) and (5) and all the terms associated with gene P_Y. We find experimentally and numerically that the transcriptional activation reaction is much faster than the other reactions involved in the reaction network. Since (6) is asymptotically stable, we used a quasi-steady state approximation to replace the value of P_Z^+ by its quasi-steady-state approximation. Moreover, as the RNA dynamics is much faster than the protein dynamics [6], and (1), and (7) are asymptotically stable, a similar approximation was used to model the synthesis of X and Z using single reactions for each. This leads to:

$$\dot{X} = \beta_X' P_X - \delta_X X, \tag{9}$$

$$\dot{Z} = \beta_Z' P_Z^+ - \delta_Z Z, \tag{10}$$

$$\bar{P_Z^+} = \frac{\bar{X}}{\bar{X} + \frac{\nu}{\omega}} P_Z^{tot}. \tag{11}$$

Here, $\beta_X' = \frac{\beta_X \alpha_U}{\delta_U}$, $\beta_Z' = \frac{\beta_Z \alpha_W^+}{\delta_W}$ and bar ($\bar{}$) denotes a steady-state value. Using, (9), (10) and (11), it can be shown that:

$$\bar{Z} = \frac{\beta_Z'}{\delta_Z} \frac{\bar{X}}{\bar{X} + \frac{\nu}{\omega}} P_Z^{tot} \tag{12}$$

where $\bar{X} = \frac{\beta_X'}{\delta_X} P_X$. Equation (12) is the steady-state value of Z and defined as a reference signal for the open-loop configuration.

2) Closed-loop steady-state output: In contrast to the open-loop configuration, in the closed-loop operation, gene P_Y is at the same concentration as gene P_Z. Now we use the same quasi-steady-state approximation to replace the ODEs of P_Y^+ and P_Z^+ by their steady-state expressions and modeling the synthesis of X and Z using single reactions for each, while keeping the two-step synthesis of Y to ensure that we consider an appropriate delay in the overall system dynamics. Moreover, assuming $\kappa XY \gg \delta_X X$ and $\kappa XY \gg \delta_Y Y$ for non-zero values of X and Y, leads to:

$$\dot{X} = \beta_X' P_X - \kappa XY, \tag{13}$$

$$\dot{V} = \alpha_V^+ X P_C - \delta_V V, \tag{14}$$

$$\dot{Y} = \beta_Y V - \kappa XY, \tag{15}$$

$$\dot{Z} = \beta_Z' X P_C - \delta_Z Z, \tag{16}$$

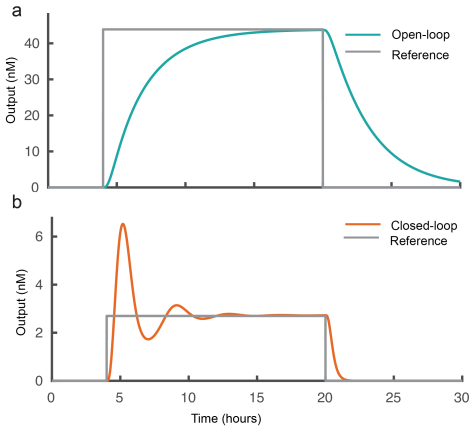

Fig. 2. Simulation results for (a) the open and (b) closed-loop operations where P_X was first increased from 0 to 0.5 nM and then decreased to 0 nM over time. The respective reference signals for the open and closed-loop operations are shown in (12) and (17). Here and elsewhere the ODE model shown in (1)-(8) was used to simulate the response of the controller with parameters shown in [6], and δ_X=δ_Y=δ_Z = 0.0001 s^{-1}. In the closed-loop case, initial P_Y^{tot} and P_Z^{tot} were 1 nM each while in the open-loop case, P_Y^{tot} was zero.

where $P_C = \frac{\omega}{\nu} P_Y^{tot} = \frac{\omega}{\nu} P_Z^{tot}$ and assuming $\frac{\nu}{\omega} \gg \bar{X}$. Using the aforementioned equations, it can be shown that:

$$\bar{Z} = \frac{\beta_Z'}{\delta_Z} \frac{\beta_X'}{\beta_Y} \frac{\delta_V}{\alpha_V^+} P_X. \tag{17}$$

Equation (17) is the steady-state value of Z and defined as a reference signal when the controller is operated in the closed-loop configuration.

3) Integral control operation: To determine an equation for $X_{FREE} = X - Y$ (13) is subtracted from (15): $\dot{X} - \dot{Y} = \beta_X' P_X - \beta_Y V$. From (14), $\bar{V} = \frac{\beta_X'}{\beta_Y} P_X$ and using this, it can be shown that: $X_{FREE} = X - Y = \beta_Y \int_0^t \bar{V} - V(\tau) d\tau$. This means that the error signal is integrated over time to correct the output concentration. This enables the controller to achieve robust reference tracking.

B. Reference tracking in closed-loop

We now sought to verify that the controller can produce an output signal as an expression from the target gene that follows the reference signal. For that, we model the response of the controller in the open and closed-loop configurations to a pulse input signal where the concentration of P_X is increased from 0 to 0.5 nM and then decreased to 0 nM over time. To determine the output response for the values of reaction parameters shown in [6], we numerically integrated the ODE model shown in (1)-(8) using the MATLAB ode23s function. Initial conditions for each molecular species are described in the figure captions.

In the absence of P_X (0 nM), expression from the target gene (P_Z) is almost zero in terms of Z concentration. In the open-loop configuration, as P_X increases from 0 to 0.5 nM, the production of X increases through the transcription of P_X and that increases the production of Z as X acts a transcriptional activator for P_Z. This results in the steady-state concentration value of the output that follows the concentration of the respective reference signal (Fig. 2a). In the closed-loop case, X acts as a transcriptional activator for both genes P_Y and P_Z. When the sequestration dominates over the degradation such that $\kappa XY \gg \delta_X X$ and $\kappa XY \gg \delta_Y Y$, some of X will be sequestered by Y, leading to a reduced amount of Z that follows the concentration of the respective reference signal (Fig. 2b). An accurate tracking means the controller should be able to follow not just a specific concentration value of the reference signal but a large dynamic range of it linearly for the same set of parameters and initial condition. Therefore, we model the steady-state output response of the controller at different concentration of P_X (0, 1, 5, 10, 15, 20, 25 and 30 nM). For each P_X value, we determined the steady-state value of Z for the open and closed-loop cases while considering the parameters shown in [6]. We found that only the closed-loop controller's output can track the reference signal linearly (Fig. 3a and b). This is due to the fact in the closed-loop configuration, Z is independent of the promoter activity of P_Z, and because of that only a limited amount of X (defined as X_{FREE}) acts a transcriptional activator such that $\frac{\nu}{\omega} \gg \bar{X}$ (17). In contrast, in the open-loop case, as the sequestration reaction is absent, Z directly depends on the promoter activity of gene P_Z which results in a nonlinear dependency of Z on X, thereby on P_X (12).

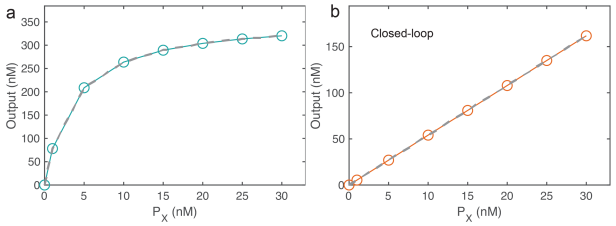

Fig. 3. Steady-state response of the controller at different concentrations of P_X (0 - 30 nM) in (a) the open and (b) closed-loop configurations. Initial concentrations of P_Y^{tot} and P_Z^{tot} were 1 nM each.

C. Closed-loop control enables disturbance rejection

Integral control provides a measure of robustness by minimizing the effect of certain kinds of disturbances on the steady-state value of the output [12]. To demonstrate this characteristic of the controller, first, we choose to perturb two kinetic parameters over time. In our controller, ω determines the activation association rate and an increase in ω increases the affinity of the activator, which leads to an increase in the steady-state concentration values of Z as long as there are enough promoter sites are available for activator to bind to genes P_Y and P_Z. Once the output reached a steady-state for the nominal value of ω, we increased ω by a factor of two as a perturbation. This results in an increased steady-state output activity in the open-loop configuration while in the closed-loop configuration, output converges to the same steady-state value (Fig. 4a). This is because an increase in ω, increases Z and also Y in the closed-loop configuration, which leads to reduce excess X through Y, and this results in reducing the production of Z. In the open-loop case, as Y is not present, an increase in ω, increases Z. We then perturb ν over time, which is the activation dissociation rate constant, and have the similar effect on Z such that the closed-loop controller can reject the effect of this perturbation on the output signal (Fig. 4b). In each case, the output is normalized

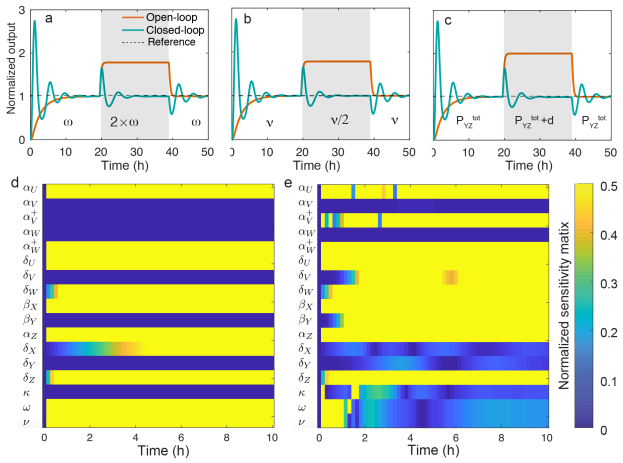

Fig. 4. **Closed-loop controller operation results in robustness to disturbances.** (a-c) Output in the presence of disturbances in (a) ω, (b) ν, and (c) in the concentrations of P_Y^{tot} and P_Z^{tot} (denoted as P_{YZ}^{tot}) where d = 1 nM. (d-g) Results of the sensitivity analysis: (d) normalized sensitivity matrix for the open-loop case and (e) the closed-loop case. The initial P_X = 0.5 nM, and P_Y^{tot} = P_Z^{tot} = 1 nM. In the open-loop case, P_Y^{tot} was zero.

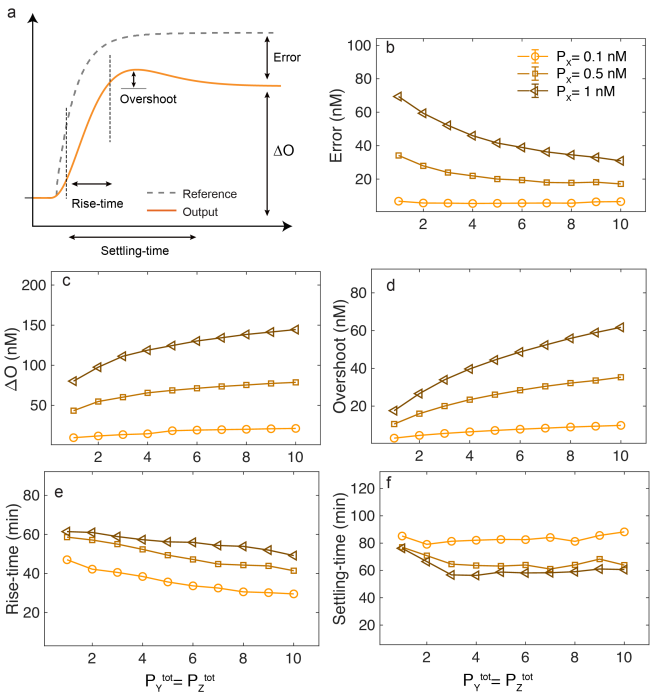

Fig. 5. **Evaluating the performance of the closed-loop controller using control theory metrics.** Five criteria were used to evaluate the controller performance. These are: steady-state error (Error) which is the absolute difference between the steady-state output and the reference signal; steady-state increase (ΔO), which is the difference between the steady-state output after and before the step change; overshoot, which is defined as the difference between the maximum and the steady-state concentration of the output; rise time, which is the time needed for the output to increase from 10% to 90% of ΔO; and finally settling time, which is the first time the output settles and stays within $\pm$5% of the steady-state output concentration. For each reaction condition, 1,000 simulations were conducted where we randomly sampled a set of parameter values from a uniform distribution. During each simulation, a step increase in P_X from 0 to 10 nM was introduced at time 10 hours. Averaged metrics of these parameters are shown here as a function of genes P_Y and P_Z concentrations.

with respect to the respective reference signal ((12) and (17) for the open and the closed-loop cases, respectively).

In the closed-loop controller, we find that the output Z is independent of the concentration of genes P_Y and P_Z (17). Therefore, adding a disturbance in the concentration of these genes should not affect the steady-state output value. To test this, we added the same amount of disturbance to P_Y^{tot} and P_Z^{tot} (denoted as d) once the output reached a steady-state value and observed that in the closed-loop configuration, the output converged to the same value (Fig. 4c).

D. Parameter sensitivity

Our next goal is to determine sensitivity of transient and steady-state response of the controller's output to parameters. Specifically, we investigate the dependency of the output on a specific set of parameters over time [8]. We perform this analysis for the controller operated in the open and the closed-loop configurations for a specific set of parameters shown in [6], and the results are shown in Fig. 4d and e respectively. Note that normalized sensitivity coefficients matrix are dependent on the time and the results indicate which parameters play the primary role in determining the transient and steady-state response of the output. We found that for the closed-loop controller, only the transient response of the output is highly sensitive to sequestration rate (κ) and the activation parameters (ω, ν) while the steady-state value of the output depends on parameters that are shown in (17).

E. Quantifying dynamic controller performance

For a comprehensive understanding of the closed-loop controller properties, we used five performance parameters (Fig. 5a), which are typically used in control theory rather than synthetic biology studies. These are the steady-state error, steady-state increase, overshoot, rise time, and settling time [13]. We then evaluated the controller performance for a step-change in P_X from 0 nM to 10 nM. To encompass a wide range of settings, we conducted 1,000 simulations with random combinations of parameters randomly from a uniform distribution within a bounded interval (upper and lower bounds of 10$\times$ and 0.1$\times$ respectively) centered around the nominal values for each reaction condition [6]. Average matrices are shown in Fig. 5. In this analysis, the cases where the output did not reach a steady-state within 5 hours were not taken into account. We found that the absolute error (Fig. 5b) is almost independent of the initial concentrations of P_Y and P_Z when P_X is low but at higher values of P_X, higher concentrations P_Y and P_Z should be preferred to reduce the error. We also observed a trade-off between the overshoot (Fig. 5d) and the rise-time (Fig. 5e) as a function of P_Y and P_Z concentrations.

F. Determining stability of the closed-loop controller

A basic requirement for a controller is to drive the system towards the desired steady-state from different initial conditions and to exert a feedback effect to cancel the influence of perturbations that knock the system out of its steady

state. This is captured by the concept of asymptotic stability of the closed-loop system. Stability analysis for nonlinear systems is typically carried out by means of Lyapunov's first and second methods for local and global stability [14]. It is known that antithetic feedback can cause sustained oscillations [7], hence stability analysis is highly pertinent. For simplicity, we ignore the reactions associated with gene P_Z as they are not actively involved in the closed-loop dynamics:

$$\dot{U} = \alpha_U P_X - \delta_U U \tag{18}$$
$$\dot{X} = \beta_X U - \kappa XY - \omega X P_Y + \nu P_Y^+ \tag{19}$$
$$\dot{V} = \alpha_V P_Y^+ - \delta_V V \tag{20}$$
$$\dot{Y} = \beta_Y V - \kappa XY \tag{21}$$
$$\dot{P}_Y^+ = \omega X P_Y - \nu P_Y^+, \tag{22}$$

Since the dynamic equation of U (18) is decoupled from the rest of the state variables, the system can be viewed as a cascade of (18) and (19)-(22). A converging-input-converging-state argument [15] can be used to reduce the stability problem of the model to that of (19)-(22) with the a constant input $\bar{U} := \alpha_U P_X / \delta_U$.

The model (19)-(22) admits a unique equilibrium (with $\bar{U} \neq 0$) which is:

$$(X_e, V_e, Y_e) = \left(\frac{\beta_X \bar{U} \delta_V (\nu/\omega)}{\beta_Y \alpha_V P_Y^{tot} - \beta_X \bar{U} \delta_V}, \frac{\beta_X \bar{U}}{\beta_Y}, \frac{P_Y^{tot} \alpha_V \beta_Y - \beta_X \delta_V \bar{U}}{\delta_V \kappa (\nu/\omega)} \right).$$

Although the equilibrium can be negative for some parameters, it is positive for the parameter regime of interest.

The model above can be reduced further by using a quasi-steady state approximation for P_Y^+, and using the fact that $\nu/\omega \gg X_e$ in the regime of interest to the following model:

$$\begin{aligned} \dot{X} &= \beta_X \bar{U} - \kappa XY \\ \dot{V} &= \beta_1 X - \delta_V V \\ \dot{Y} &= \beta_Y V - \kappa XY \end{aligned} \tag{23}$$

where $\beta_1 = \alpha_V P_Y^{tot} \omega / \nu$, and it has a unique positive equilibrium at:

$$(\bar{X}, \bar{V}, \bar{Y}) = \left(\frac{\delta_V \beta_X \bar{U}}{\beta_Y \beta_1}, \frac{\beta_X \bar{U}}{\beta_Y}, \frac{\beta_1 \beta_Y}{\delta_V \kappa} \right). \tag{24}$$

In the parameter regime of interest, the equilibria of (19)-(22) and (23) are approximately equal. This justifies the wide use of the approximate system (23) as a deterministic model for antithetic feedback [7], [16].

1) Local stability analysis: Locally stability can be studied via Lyapunov's first method.

Proposition 1: Consider (23) with any arbitrary positive parameters and positive constant input value. Then the equilibrium (24) is locally asymptotically stable, i.e the Jacobian matrix evaluated at (24) is Hurwitz.

Proof: The Jacobian evaluated at (24) is given as follows:

$$\begin{bmatrix} -\beta_Y \beta_1 / \delta_V & 0 & -\kappa \delta_V \beta_X \bar{U} / (\beta_Y \beta_1) \\ \beta_1 & -\delta_V & 0 \\ -\beta_Y \beta_1 / \delta_2 & \beta_Y & -\kappa \delta_V \beta_X \bar{U} / (\beta_Y \beta_1) \end{bmatrix}.$$

We need to verify that all eigenvalues have negative real parts. The characteristic equation is:

$$s^3 + \left(\frac{\beta_1 \beta_Y}{\delta_V} + \delta_V + \frac{\kappa \beta_X \bar{U} \delta_V}{\beta_1 \beta_Y} \right) s^2 + \left(\beta_1 \beta_Y + \frac{\delta_V^2 \kappa}{\beta_1 \beta_Y} \right) s + \delta_V \kappa \beta_X \bar{U} = 0$$

Computing the first column in the Routh-Hurwitz criterion [17], the problem reduces to verifying that $(B + \frac{\delta_V A}{B})(\frac{B}{\delta_V} + \frac{A}{B \delta_V}) > A$, where $A := \delta_V \kappa \beta_X \bar{U}, B := \beta_1 \beta_Y$. This is equivalent to $B(\frac{B}{\delta_V} + \delta_V) + (\frac{1}{\delta_V} + \frac{\delta_V^2}{B})A + \frac{A^2}{B^2} > 0$. The last inequality holds for any $A, B, \delta_V > 0$. ■

2) Global stability via a sum-of-square search: In this subsection we discuss building Lyapunov functions for the reduced system (23) and the original system (19)-(22). Despite its simplicity, global stability analysis of (23) is not straightforward. In fact, a similar system [7] has been shown to exhibit a limit cycle despite the local stability of the unique steady state. Nevertheless, since we have the parameters in [6], we can perform a Lyapunov function search using sum-of-square (SOS) methods [18], [19]. The basic idea is to replace the polynomial inequalities with their sum-of-square relaxations. Introducing $z := [X - \bar{X}, V - \bar{V}, Y - \bar{Y}]^T$, let us write (23) as $\dot{z} = f(z)$. We are looking for a polynomial Lyapunov function $V(z)$ with specified monomials and unknown coefficients that satisfies the following:

$$\begin{cases} V(z) & \geq (z_1^2 + z_2^2 + z_3^2) \\ -\frac{\partial V}{\partial z} f(z) & \geq 0 \end{cases},$$

where the first inequality is equivalent to V being positive definite and vanishing only at $(0,0,0)$. The second inequality is equivalent to $\dot{V}(z(t)) \leq 0$. We can also add $z_1^2 + z_2^2 + z_3^3$ to the second inequality to force $\dot{V}$ to vanish at (0,0,0) only.

However, polynomial inequalities are hard to solve in general. Hence, we look for an SOS relaxation that certifies the positivity of the required polynomials. For a polynomial $p(x)$, this means finding a matrix $Q \geq 0$ such that $p(x) = Z(z)^T Q Z(z)$ for an appropriate monomial vector $Z(z)$. Let L be the Cholesky matrix such that $L^T L = Q$. Hence $p(x) = (LZ(z))^T (LZ(z))$ is a sum of squared polynomials which certifies positivity. In the context of finding a Lyapunov function, this means finding two positive definite matrices $Q_1, Q_2 \geq 0$ such that

$$\begin{cases} V(z) - (z_1^2 + z_2^2 + z_3^2)) & = Z(z)^T Q_1 Z(z) \\ -\frac{\partial V}{\partial z} f(z) & = Z(z)^T Q_2 Z(z). \end{cases},$$

where $Z(z)$ is a vector of monomial that is chosen according to the form of $V(z)$. Since the problem is affine in the unknowns, the problem can be re-written as a semi-definite program (SDP) and solved using available solvers. This process has been automated via the MATLAB package SOSTOOL [20], which we have used. In particular, a *fourth-order* Lyapunov function can be constructed for any given P_X, P_Y^{tot}. Fig. 5 plots the level surface of the Lyapunov function.

It is undesirable to compute the Lyapunov function for each copy number values P_X, P_Y^{tot}. In order to certify stability for all $P_X, P_Y^{tot} \geq 0$ we will use a Positivstellensatz-based approach [21], [18], [19]. Consider the system $\dot{z} = f(z, P_X, P_Y^{tot})$.

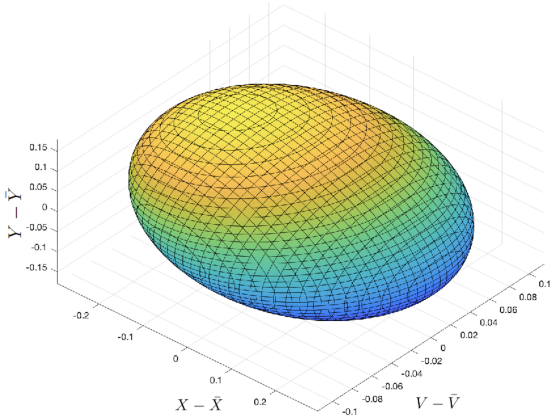

Fig. 6. The level surface for $V(x)=2$ for the quartic Lyapunov function constructed for the system (23) with $P_Y^{tot}=P_X=0.7\,n$M. It can also be interpreted as a trapping set for the system. This means that any trajectory that starts inside it cannot leave.

Our aim is to find a Lyapunov function $V(z,P_X,P_Y^{tot})$ that satisfies the positivity and the nonincreasingness condition *whenever* $P_X,P_Y^{tot}>0$. This can be written equivalently as certifying the emptiness of an appropriate semi-algebraic set. In particular, we need to find four SOS polynomials $s_1(z),s_2(z),s_3(z),s_4(z)$ (with specified monomials) that satisfy the following:

$$\begin{cases} V(z)-s_1(z)P_X-s_2(z)P_Y^{tot}-(z_1^2+z_2^2+z_3^2) & \text{is SOS} \\ -P_Y^{tot}\frac{\partial V}{\partial z}f(z,P_X,P_Y^{tot})-s_3(z)P_X-s_4(z)P_Y^{tot} & \text{is SOS.} \end{cases},$$

Note that the second inequality multiplies by P_Y^{tot} since it appears in the denominator in the original inequality. Solving the associated SDPs, we have successfully constructed a fourth-order Lyapunov function that certifies global stability for all $P_X,P_Y^{tot}>0$ with the parameters given in [6], which is not shown here due to the lack of space.

II. CONCLUSIONS AND FUTURE WORK

In this work, we mathematically investigated the operation of our biomolecular integral controller for effective and robust gene expression regulation. We demonstrated that the controller could not only track the reference signal over a wide range of conditions, but it can also reject perturbations introduced to the output, due to disturbances in kinetic parameters when operated in the closed-loop configuration. These characteristics illustrate the advantage of having an effective sequestration reaction to realize closed-loop operation. Moreover, using the estimated parameters, we have constructed Lyapunov functions that proved global stability for any initial reaction condition. Work in progress concerns the extension of this approach to establish global stability for all possible parameters.

The robust and reliable operation of the closed-loop controller suggests that other biochemical reactions might be used to implement alternative closed-loop integral controllers that can precisely regulate other biologically relevant molecules.

III. ACKNOWLEDGMENTS

This material is based upon work supported by the DARPA FA8650-18-1-7800, DARPA HR0011-16-C-01-34, NSF 1716623, and AFOSR FA9550-14-1-0060.

REFERENCES

[1] H. El-Samad, J. P. Goff, and M. Khammash, "Calcium homeostasis and parturient hypocalcemia: An integral feedback perspective," *Journal of Theoretical Biology*, vol. 214, no. 1, pp. 17–29, 2002.
[2] D. Del Vecchio and R. M. Murray, *Biomolecular feedback systems*. Princeton University Press Princeton, NJ, 2015.
[3] M. J. Dunlop, J. D. Keasling, and A. Mukhopadhyay, "A model for improving microbial biofuel production using a synthetic feedback loop," *J Systems and biology, synthetic*, vol. 4, no. 2, pp. 95–104, 2010.
[4] N. Barkai and S. Leibler, "Robustness in simple biochemical networks," *Nature*, vol. 387, no. 6636, pp. 913–7, 1997.
[5] K. J. Astrm and R. M. Murray, *Feedback systems: an introduction for scientists and engineers*. Princeton university press, 2010.
[6] D. Agrawal, R. Marshall, V. Noireaux, and E. D. Sontag, "In vitro implementation of robust gene regulation in a synthetic biomolecular integral controller," *bioRxiv*, 2019. [Online]. Available: https://www.biorxiv.org/content/early/2019/01/20/525279
[7] C. Briat, A. Gupta, and M. Khammash, "Antithetic integral feedback ensures robust perfect adaptation in noisy biomolecular networks," *Cell systems*, vol. 2, no. 1, pp. 15–26, 2016.
[8] D. K. Agrawal, X. Tang, A. Westbrook, R. Marshall, C. S. Maxwell, J. Lucks, V. Noireaux, C. L. Beisel, M. J. Dunlop, and E. Franco, "Mathematical modeling of rna-based architectures for closed loop control of gene expression," *J ACS synthetic biology*, vol. 7, no. 5, pp. 1219–1228, 2018.
[9] E. Franco, G. Giordano, P. O. Forsberg, and R. M. Murray, "Negative autoregulation matches production and demand in synthetic transcriptional networks," *ACS Synth Biol*, vol. 3, no. 8, pp. 589–99, 2014.
[10] V. Hsiao, E. L. de los Santos, W. R. Whitaker, J. E. Dueber, and R. M. Murray, "Design and implementation of a biomolecular concentration tracker," *ACS Synth Biol*, vol. 4, no. 2, pp. 150–61, 2015.
[11] E. Sontag, "Adaptation and regulation with signal detection implies internal model," *Systems Control Lett.*, vol. 50, no. 2, pp. 119–126, 2003.
[12] J. Huang, A. Isidori, L. Marconi, M. Mischiati, E. Sontag, and W. M. Wonham, "Internal models in control, biology and neuroscience," *2018 Ieee Conference on Decision and Control (Cdc)*, pp. 5370–5390, 2018.
[13] E. D. Sontag, *Mathematical Control Theory: Deterministic Finite Dimensional Systems*. Springer Science & Business Media, 2013, vol. 6.
[14] H. K. Khalil, *Nonlinear Systems*, 3rd ed. Prentice Hall, 2002.
[15] E. D. Sontag, "A remark on the converging-input converging-state property," *IEEE Transactions on Automatic Control*, vol. 48, no. 2, pp. 313–314, 2003.
[16] Y. Qian and D. Del Vecchio, "Realizing 'integral control' in living cells: how to overcome leaky integration due to dilution?" *Journal of The Royal Society Interface*, vol. 15, no. 139, p. 20170902, 2018.
[17] R. C. Dorf and R. H. Bishop, *Modern control systems*. Pearson, 2011.
[18] P. A. Parrilo and S. Lall, "Semidefinite programming relaxations and algebraic optimization in control," *European Journal of Control*, vol. 9, no. 2-3, pp. 307–321, 2003.
[19] G. Chesi, "LMI techniques for optimization over polynomials in control: a survey," *IEEE Transactions on Automatic Control*, vol. 55, no. 11, pp. 2500–2510, 2010.
[20] S. Prajna, A. Papachristodoulou, and P. A. Parrilo, "Introducing sostools: A general purpose sum of squares programming solver," in *Proceedings of the 41st IEEE Conference on Decision and Control, 2002.*, vol. 1. IEEE, 2002, pp. 741–746.
[21] G. Stengle, "A nullstellensatz and a positivstellensatz in semialgebraic geometry," *Mathematische Annalen*, vol. 207, no. 2, pp. 87–97, 1974.